

HOW UNIFORM IS TEV-BLAZAR HEATING?

ASTRID LAMBERTS¹, PHILIP CHANG¹, EWALD PUCHWEIN², CHRISTOPH PFROMMER³, AVERY E. BRODERICK^{4,5} AND MOHAMAD SHALABY^{2,3,6}

¹ Department of Physics, University of Wisconsin-Milwaukee, 1900 East Kenwood Boulevard, Milwaukee WI 53211, USA

² Institute of Astronomy and Kavli Institute for Cosmology, University of Cambridge, Madingley Road, Cambridge, CB3 0HA, UK

³ Heidelberg Institute for Theoretical Studies, Schloss-Wolfsbrunnenweg 35, D-69118 Heidelberg, Germany

⁴ Perimeter Institute for Theoretical Physics, 31 Caroline Street North, Waterloo, ON, N2L 2Y5, Canada

⁵ Department of Physics and Astronomy, University of Waterloo, 200 University Avenue West, Waterloo, ON, N2L 3G1, Canada and

⁶ Department of Physics, Faculty of Science, Cairo University, Giza 12613, Egypt

Draft version September 10, 2014

ABSTRACT

TeV-blazars heat up the intergalactic medium (IGM) as the gamma-rays they produce turn into pairs which lose their kinetic energy to the surrounding medium through plasma instabilities. Assuming uniform heating, this mechanism increases the temperature of the IGM and produces an inverted temperature-density relation in underdense regions. This additional heating source significantly impacts large scale structure formation. In this paper we want to go beyond the approximation of uniform heating and quantify the heating rate fluctuations and their impact on the thermal history of the IGM. We analytically compute a filtering function relating the heating rate fluctuations to the underlying dark matter density field. We implement it in the cosmological code GADGET-3 and perform large scale simulations to determine the impact of inhomogeneous heating. We show that, because of the bias, blazar heating is inhomogeneous, especially at high redshift. The temperature-density relation shows an important scatter at $z \geq 2$. At lower redshift, the average temperature of the IGM is lower than in the uniform case. We find that blazar heating is more complex than initially assumed and that the temperature-density relation is not unique. Future work will deal with the observational impact and large scale structure formation in this context. Our analytic model for the heating rate fluctuations couples well with large scale simulations and provides a cost-effective alternative to subgrid models.

Subject headings: BL Lacertae objects: general, cosmology: theory, gamma-rays: general, intergalactic medium, large-scale structure of universe

1. INTRODUCTION

The intergalactic medium is an ionized medium which relates galaxies and clusters together, thus forming the cosmic web (Bond et al. 1996). It constitutes the main reservoir of baryons available for the formation of collapsed objects such as galaxies and clusters (Rauch et al. 1997). Observations of metal-enriched materials (see e.g. Simionescu et al. (2009); Werner et al. (2010)) prove its evolution due to already formed stars and galaxies. This close relation between the IGM and structure evolution makes it a crucial aspect for the understanding of large scale structure in the universe.

The temperature of the IGM is mostly set by photoionization of hydrogen and helium, competing with adiabatic cooling. This yields a slowly cooling universe, with denser regions being warmer because more resistant to adiabatic cooling. Observations of absorption lines in spectra of background quasars due to neutral gas confirm this equation of state (Schaye et al. 2000; Ricotti et al. 2000; Rudie et al. 2012). However, recent measurements found that underdense regions may be warmer than expected (Viel et al. 2009; Bolton et al. 2008; Boera et al. 2014). Although an inverted temperature-density relation in underdense regions has not been firmly established yet (Bolton et al. 2014), the recent observations suggest the thermal history of the IGM is more complex than initially assumed.

Broderick et al. (2012) recently described a complementary heating mechanism, through TeV blazars. TeV blazars are active galactic nuclei emitting very high energy gamma rays (VHEGR, $E \geq 100$ GeV). About 50 of these sources have been discovered so far (<http://tevcat.uchicago.edu/>), by the space-based *Fermi*/LAT and ground based Cerenkov telescopes such as MAGIC, H.E.S.S. and VERITAS. The universe is mainly opaque to VHEGR, as they interact with the extragalactic background light (EBL) producing electron/positron pairs (Gould & Schréder 1967; Stecker et al. 1992). It is commonly assumed that the electron/positron pairs then upscatter photons of the cosmic microwave background, resulting in a halo of photons with energies between .1 and 100 GeV. Such extended emission around TeV blazars has not been observed so far (Aleksić et al. 2010; H. E. S. S. Collaboration et al. 2014), which is interpreted by deviations due to the intergalactic magnetic field (IGMF) (Durrer & Neronov 2013; Vovk et al. 2012; Dermer et al. 2011). Broderick et al. (2012) showed that the pair beams rather transfer their energy directly to the IGM through plasma instabilities.

The pairs constitute a dilute, ultrarelativistic beam, which is subject to several plasma instabilities, from which the “oblique” instability (Bret et al. 2004) is the most powerful. Assuming its efficiency in the linear regime extends to the non-linear regime, Chang et al. (2012) (hereafter PaperI) show it is responsible for increasing the temperature of the IGM by almost a factor

10 in low density regions. While this assumption is still debated (see Miniati & Elyiv (2013); Sironi & Giannios (2014) but also Saveliev et al. (2013); Schlickeiser et al. (2013, 2012), Chang et al, submitted), throughout all this paper we will assume plasma instabilities are the dominant mechanism for cooling of the pair beams.

Including TeV blazar heating in the thermal history of the IGM, Chang et al. (2012) were able to reproduce the inverted temperature-density relation for low density regions. In a follow-up paper, Pfrommer et al. (2012) found that TeV blazar heating is responsible for creating a redshift dependent entropy floor in clusters and galaxies, thus suppressing the formation of dwarf galaxies after the peak of blazar activity at redshift $z \simeq 2$ and providing an explanation to the “missing satellite problem” (Kravtsov 2010). Implementing volumetric, i.e. uniform, blazar heating in a hydrodynamical simulation of galaxy formation, Puchwein et al. (2012) find excellent agreement with the one and two-point statistics of the Ly α forest, main tracer of low density regions in the universe.

At the present epoch, as the mean separation between visible blazars is smaller than the mean free path for pair creation, blazar heating can be considered as uniform, **at least at low redshifts**. However, it is natural to expect a larger TeV flux close to higher density regions where visible structures form. The goal of this paper is to go beyond the hypothesis of uniform heating and to link TeV blazar heating to the underlying clustered density field and take into account the bias of sources. We expect the heating to be uniform at scales of order of the mean free path for pair creation (about 35 Mpc at the present day) and inhomogeneities to appear at larger scales.

Self-consistently studying the evolution of the IGM from first principles involves modeling both the formation and evolution of galaxies and the largest scales of the universe. As this is still far beyond reach of current computers, we have determined a filter function which relates the heating fluctuations to the dark matter structure similarly to Pritchard & Furlanetto (2007); Barkana & Loeb (2005); Pontzen (2014). Based on the hierarchical structure formation in a Λ CDM universe, it naturally selects the relevant lengthscales for TeV blazar heating (§2). We have implemented it in large scale cosmological simulations (§3). We focus on equation of state and thermal evolution of the IGM (§ 4). We then discuss how this heating mechanism compares to other feedback mechanisms and impacts large scale structure formation (§5) and conclude (§6).

2. DETERMINING THE WINDOW FUNCTION

2.1. *Intuitive understanding*

One zone models (Chang et al. 2012; Pfrommer et al. 2012) and numerical simulations (Puchwein et al. 2012) of blazar heating on the IGM assume that the heating is uniform. Because the heating rate depends on the local density of EBL and TeV photons, the assumption of uniform heating implies that the distributions of EBL and TeV photons are uniform. For EBL photons, this is likely the case, as the mean free path is larger than the Hubble length. However for TeV photons the mean free path compares with the separation between TeV sources for $z \geq 1$, so the *spatial* fluctuations in the heating rate are

likely nontrivial. Moreover, the sources of TeV photons tend to be clustered and so the IGM near these clustered regions will get an increased flux of photons due to both a $1/r^2$ increases as well as an increased number of sources.

Our goal is to include a more realistic model for heating due to TeV blazars in numerical simulations. To properly calculate the heating fluctuations due to TeV blazar heating, the formation and evolution of accreting supermassive black holes must be modeled in a full self-consistent cosmological simulation. In addition, the TeV radiation from these systems must be ray-traced through the simulation volume. Such a task is computationally intractable. As a result, we have elected to model this TeV blazar heating in a more statistical manner.

We assume that TeV blazars are associated with galaxies and that they roughly emit over 4π steradian. The latter assumption remains valid so long as the number of TeV blazars is large enough such that every spot in the universe is **at least** illuminated by **at least** a few TeV blazars. The heating rate at a given point \mathbf{x} is determined by the received TeV flux from all the sources within a certain radius r_{max} , where $r_{max} \gg$ the mean free path of VHEGRs

$$\dot{q}(\mathbf{x}) = \frac{1}{4\pi} \int_{\Omega} \int_0^{r_{max}} \mathcal{E}(\mathbf{r}' + \mathbf{x}) \sigma e^{-\tau} d\Omega dr', \quad (1)$$

\mathcal{E} is the emissivity of the sources (energy per unit time, per unit volume). σ (in cm^{-2}) is the energy-averaged cross section for pair production on the extragalactic background light and τ is the associated optical depth along the line of sight.

One can then express the emissivity as a mean value and a first order correction. The TeV emissivity is related to the presence of a supermassive black holes at centers of galaxies, which cluster in overdense regions. We can also relate the overdensity of galaxies to the dark matter overdensities. On average, larger overdensities contain larger number of galaxies (reflected in their bias) and hence are more prominent sources of TeV emission. In this manner, we compute the fluctuations of TeV blazar heating in a statistical sense.

To show this more explicitly, we begin by expressing the heating rate \dot{q} as a mean heating rate $\bar{\dot{q}}$ plus a small fluctuation δ_H .

$$\dot{q} = \bar{\dot{q}}(1 + \delta_H). \quad (2)$$

with ρ the local density and $\bar{\rho}$ its average over the whole region. The method is based on a Taylor expansion of the quantities describing the TeV sources and keeping only the first order corrections in Fourier space. We thus have

$$\tilde{\delta}_H = \tilde{W}_H \tilde{\delta}, \quad (3)$$

where \tilde{W}_H is defined as the window function and maps the Fourier transform of the overdensity, $\tilde{\delta}$, to the Fourier transform of the heating fluctuations, $\tilde{\delta}_H$. This naturally yields the significant lengthscales for heating fluctuations. The detailed exposition of this method, in the Newtonian limit and in an expanding universe, is given in Appendix A. In the following section, we present the general method and highlight the underlying hypotheses of our work.

2.2. Window function for TeV blazar heating

To determine the heating rate fluctuations we express the TeV emissivity in Eq. 1 as a mean value and a first order correction. The heating rate at a given point is set by the received TeV flux from all the sources within a certain radius. We assume that the pairs lose their energy to the IGM at the point where they are created. As stated in Broderick et al. (2012), this is a reasonable assumption as the plasma instability lengthscales are significantly smaller than the mean free path of these TeV photons. The heating also depends on the rate at which the TeV photons are converted into pairs and that pairs lose their energy to the surrounding medium. Assuming all the energy of the pairs is converted into heat at the location where they are created.

The TeV emissivity relates to the presence of a supermassive black holes at centers of galaxies, which cluster in overdense regions. Matter is tightly coupled to the underlying dark matter, which evolution is easy to model analytically within the linear approximation. The linear approximation is valid as long as the overdensity is small, which is true in the early universe and then breaks down at small scales as very dense structures form. Our computation takes into account the bias between baryonic matter and dark matter (Mo & White 1996), as we detail in §???. To model cosmic distances, Eq. 1 is integrated in redshift space and we take into account the resulting energy loss for the TeV photons as well as the first order corrections due to proper motions of the sources within the Hubble flow (Kaiser 1987). We integrate over the energy distribution of the TeV-emission . We thus get

$$\tilde{W}_H(k, z) = \frac{1}{\bar{X}} \int_{E_{min}}^{E_{max}} dE \int_z^{z_{max}} \frac{dX(E, z, z')}{dz'} \times \frac{D(z')}{D(z)} \left((b(z) + 1)j_0(kr) - \frac{2}{3}j_2(kr) \right) dz', \quad (4)$$

with

$$X(E, z', z) = \frac{e^{-\tau(z, z', E)}(1+z)^2}{H(z')\epsilon(E', z')}. \quad (5)$$

and \bar{X} its spectral average. E is the energy of the received TeV photon and, E' its initial energy and ϵ the (comoving) blazar luminosity density. b is the bias and j_0 and j_2 spherical Bessel functions.

Assuming the TeV blazar distribution follows the redshift evolution of quasars, Broderick et al. (2012) determined the blazar luminosity density in the TeV band based on a fit to Hopkins et al. (2007)

$$\begin{aligned} \mathcal{E}(E', z) &= \mathcal{E}(E', z=0)\Phi_B(z) \\ &\simeq \zeta\epsilon(E', z=0)\Phi_Q(z), \end{aligned} \quad (6)$$

with $\zeta = 2.1 \times 10^{-3}$ and

$$\Phi_Q(z) = 10^{-0.0037(1+z)^4 + 0.085(1+z)^3 - 0.0778(1+z)^2 + 2.795(1+z) - 2.133}. \quad (7)$$

As the spectra of TeV blazars follow a power law with intrinsic (i.e. redshift corrected) spectral index α , one has

$$\epsilon(E', z=0) = \epsilon(E_0, z=0) \left(\frac{E'}{E_0} \right)^{-\alpha} \equiv \epsilon_0 \left(\frac{E'}{E_0} \right)^{-\alpha}, \quad (8)$$

with $\epsilon_0 = (1.7 - 4.8) \times 10^{-36} \text{ erg s}^{-1} \text{ cm}^{-3}$ the current blazar luminosity density. Using 28 TeV blazars, Chang et al. (2012) find that $\alpha \simeq 3$ and $E_0 \simeq 1 \text{ TeV}$. Following the emission of the nearest TeV blazars, we use $E_{min} = 100 \text{ GeV}$, and $E_{max} = 10 \text{ TeV}$. Assuming blazars follow a similar evolution to quasars, we use $z_{max} = 5$ (Hopkins et al. 2007).

The optical depth is set by the mean free path $D_{pp}(E', z)$ of TeV photons before they interact with an EBL photon and produce an electron-positron pair. Its redshift evolution is set by the EBL and is hard to constrain as it is related to the star formation history of the universe as well as its metalicity and dust contents (see e.g Franceschini et al. (2008); Stecker et al. (2006)). Following Chang et al. (2012) we use a prescription

$$D_{pp}(E, z) = 35 \left(\frac{E}{1 \text{ TeV}} \right)^{-1} \left(\frac{1+z}{2} \right)^{-\xi} \text{ Mpc}, \quad (9)$$

where $\xi = 4.5$ for $z < 1$ and $\xi = 0$ for $z > 1$ (Kneiske et al. 2004; Neronov & Semikoz 2009). The proper mean free path is constant for $z \geq 1$, however, the comoving mean free path increases for increasing redshift.

The TeV flux fluctuations are related to the distribution of blazars, which is biased with respect to the distribution of dark matter halos (Mo & White 1996). Luminous structures such as galaxies or clusters preferentially populate the high peaks of the dark DM density distribution. The bias of a certain structure is the ratio between its power spectrum to the power spectrum of the DM halos (see e.g. (Cooray & Sheth 2002) for a review). The bias is the strongest for the more massive objects, such as quasars. Due to the TeV photon absorption, there is no observation of TeV blazar bias. As blazars are supermassive black holes, an estimate can be obtained from quasar bias. However, blazars have lower accretion rates than quasars, and may trace less clustered environments such as regular galaxies. Therefore, we perform simulations with both an estimate for quasar bias and galaxy bias, a model with blazar bias will probably lay somewhere in between. We use fits to Basilakos et al. (2008) for both our galaxy and quasar bias model. They correspond to a halo mass of $10^{12} h^{-1} M_\odot$ and $10^{13} h^{-1} M_\odot$ respectively. The quasar model is based on 2dF (Croom et al. 2005), SDSS DR4 (Myers et al. 2007) and SDS DR5 data for the highest redshift (Shen et al. 2007). The galaxy bias model uses optical data from the VIMOS VLT (Marinoni et al. 2005) and Subaru deep filed data (Kashikawa et al. 2006). In all cases, it is important to keep in mind the uncertainties on the measurements of the bias, especially at high redshift.

Using Eqs. 6 and 9 in Eq. 4 then gives the complete window function for TeV blazar heating as shown

of Fig. 1 for $z = 1, 2$ and 4 for a model with galaxy and quasar bias. We have computed the window function using an embedded Runge-Kutta method which is able to capture the fast variation of the Bessel functions at large wavenumbers while decreasing computing time at smaller wavenumbers. To avoid unnecessary computations, we set both Bessel functions to zero when kr is larger than 50 . We checked this does not affect the final result.

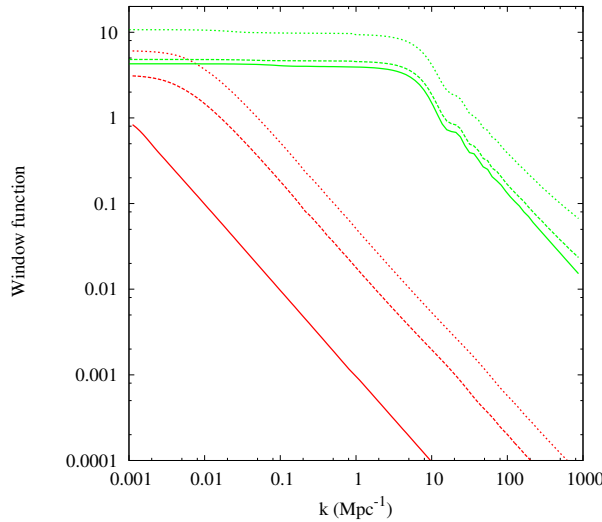


FIG. 1.— Window function for TeV blazar heating from $z=1$ (solid lines), $z=2$ (dashed lines) and $z=4$ (dotted line) for the galaxy bias model (red) and the quasar bias model (green).

The window function describes how density fluctuations translate into heating fluctuations. **The quasar bias model has more power at all scales because of the larger bias. For the galaxy model, at high redshift, most of the power resides in the large scales, meaning blazar heating traces the density fluctuations. At smaller scales, density fluctuations have no impact and blazar heating is uniform. At the current epoch, the TeV blazar heating is uniform as the heating fluctuations trace density fluctuations at scales larger than 100 Mpc, where the Universe is essentially uniform (see Clowes et al. (2013) and references therein). For the quasar model, there is much more power at small scales and small scale density fluctuations will lead to enhanced heating.** As the window function remains positive at all scales, underdense regions such as voids are the only areas where a lower than average heating rate is expected. Above average heating is possible in large scale overdensities but also at smaller scales when the overdensity is important. However, in such regions the linear theory for the dark matter evolution breaks down and we will not consider such cases. After these first analytic estimates, we include the window function to model TeV blazar heating in cosmological simulations. Comparison with Fig. 8, computed without bias, shows that galaxy bias is responsible for values above unity in the window function as it takes into account clustering

of matter.

3. NUMERICAL METHOD

3.1. Cosmological simulations

We perform simulations with the smoothed particle hydrodynamics (SPH) code P-GADGET 3, an upgraded version of the publicly available GADGET-2 code (Springel 2005). The code solves the gravitational evolution of both dark matter and gas particles following a TreePM N-body method. The hydrodynamical evolution of the gas is modeled using an entropy conserving scheme (Springel & Hernquist 2002).

To ease comparison with simulations with uniform blazar heating, we use a very similar setup to Puchwein et al. (2012), which we briefly summarise here.— The cosmological model is based on the WMAP 7-year data (Komatsu et al. 2011): $\Omega_M = 0.272$, $\Omega_\Lambda = 0.728$, $\Omega_B = 0.0465$, $h = 0.704$ and $\sigma_8 = 0.809$. The initial conditions were evolved from $z = 100$ until $z = 1$ in boxes with comoving side lengths of 100 and $500 h^{-1}$ Mpc and periodic boundary conditions. ALcIn the 100 Mpc box, we use 2×256^3 particles, which gives a mass of $m_{gas} = 3.9 \times 10^{8h^{-1}} M_\odot$ and $m_{DM} = 2 \times 10^9 h^{-1} M_\odot$ for baryonic and dark matter particles, respectively. We used a gravitational softening length of $80 h^{-1}$ kpc. *These numbers will be updated as I determine the minimal resolution needed and I have a plot to prove it.*

A subgrid model (Springel & Hernquist 2003) accounts for radiative cooling, star formation and supernova feedback. As we are only interested in the low density intergalactic medium, we use a simplified model for star formation which significantly speeds up the simulations. In this model, gas particles with $\delta \geq 1000$ and $T \leq 10^5$ K are directly converted into stars (Viel et al. 2004). Although it results in unrealistic galaxy properties, this approximation does not affect regions with $\delta \leq 0$. Black hole feedback other than TeV blazar heating is not included. Photoheating is set by ionization equilibrium in the presence of an external UV field, which parameters are set by Faucher-Giguère et al. (2009). In this model, reionization happens too fast to allow efficient heating. Following Puchwein et al. (2012) we thus include the equivalent heat input by hand at redshift $z = 10$.

The size of the box is set to model the heating perturbations on the scales determined by the window function in Fig.1. We want to model a representative cosmic sample and probe distances far beyond the mean free path of the TeV photons, which is of order of 35 (comoving) Mpc at $z=0$ (but 100 Mpc at $z=2$). **We perform most of our simulations in a $L_{box}=100 h^{-1}$ Mpc box and perform an additional simulation with $L_{box} = 500 h^{-1}$ Mpc to capture all the significant lengthscales and include large clusters in our simulation.** At this scale, refined modeling of the evolution of small scale structure such as galaxies is computationally prohibitive. Our approach is similar to the modeling of the epoch of re-ionization *cite someone, justify low resolution*.

3.2. Including the TeV blazar heating fluctuations

We model the impact of the fluctuations in TeV blazar heating on the thermodynamics of the IGM. For every gas particle, the blazar heating is set by the mean value plus some correction depending on the local density field (Eq. 2). As in Puchwein et al. (2012), we adopt the mean heating rate computed by Chang et al. (2012) (Eq. 6).

~~based one a one-zone model of the thermal evolution of the IGM.~~ We focus on the model with “intermediate” values for the blazar heating., where

Modeling fluctuations by implementing a filtering function in a large scale simulation is a totally new method. The computation of the fluctuations is done in Fourier space and is inspired by the resolution of the Poisson equation. The Fourier transforms are performed with the parallel extension of the FastFourierTransform Library. The first step is map the particles onto a mesh, which is done with a clouds-in-cells algorithm (Hockney & Eastwood 1981). Then, we determine the Fourier transform of the DM only density field. Then the density field is multiplied by the window function performing a bilinear interpolation of tabulated values for certain values of redshift and wavenumber. In this paper we used 20 **equally logarithmically** spaced redshift bins from $z = 5$, where blazar heating turn on, until the end of the simulation. We used 256 wavenumber bins. We also deconvolve for the clouds-in-cells kernel by dividing by $\text{sinc}^2(k_x L/2N)\text{sinc}^2(k_y L/2N)\text{sinc}^2(k_z L/2N)$. We then perform the inverse Fourier transform and renormalize. The last step is to remap the results onto the gas particles **only**.

Talk about the number of particles and resulting mass and softening length here.

4. RESULTS

Fig. 2 shows the heating rate fluctuations in the mid-plane of the $L_x = 100$ Mpc simulation for $z = 4, 3, 2, 1$. The corresponding density field is shown in the left column and shows increasing structure formation as the redshift decreases. The heating map has a linear scale while the density scale is logarithmic. The heating rate fluctuations are, on average, much smaller than the density fluctuations. This is because the window function filters out small scales, which correspond to collapsed regions, where density fluctuations are the highest. To the zeroth order, one can thus consider TeV blazar heating to be uniform, as was assumed in PaperI.

Additional heating (i.e. $\delta_H > 0$) occurs around clustered regions. This is expected, as, especially at high redshift, the window function translates large scale density fluctuations into heating rate fluctuations. Conversely, underdense regions, such as the large void around $x = 60, y = 70$ display below average heating as they are isolated from sources, which flux decreases as r^{-2} . As the redshift decreases, the heating rate becomes more and more uniform as almost the whole volume has been heated by an increasing number of sources.

Fig. 3 shows the ratio of the internal energy due to blazar heating with respect to the total internal energy. These maps clearly highlight that blazar heating has more impact in underdense regions, as the heating rate per baryon is higher. Even if these regions receive less heat than regions with higher density (see Fig. 2), blazar heating can account to up to 10% of the total internal energy. This effect increases with time, as structures

grow, the dense regions get denser and the voids get less dense. The ratio between the blazar induced energy and total energy first increases over time and then decreases between $z = 2$ and $z = 1$. This evolution is related to the blazar luminosity evolution, which peaks at $z=2$ (PaperI).

Blazar heating preferentially affects underdense regions, and this is visible on the temperature density relation shown on Fig. 4. The colormap shows the mass weighted $T - \rho$ relation from our simulations and the grey contours show the case for uniform blazar heating **with the same resolution (Puchwein et al. 2012)**. When the clustering is taken into account, the temperature-density relation has a significant scatter for underdense regions**especially when we use the quasar bias model, due to increased clustering of the sources**. For the quasar bias model, this scatter results in the lower envelope of the temperature-density relation to change little from the case with no blazar heating. However, the mean temperature is very close to the uniform blazar heated case. At $z = 1$ the simulation with the galaxy bias model has a very similar outcome to the uniform model and blazar heating can be considered as homogeneous, though the lower envelope sits at a lower temperature. **The scatter decreases with redshift as all regions of the universe have been affected by at least on TeV blazar. The temperature shows the impact of blazars integrated over time, and thus asymptotically tends to the uniform case. In both models, deviations from the uniform case become significant at $z \leq 3$.**

Fig. 5 shows the mass-weighted probability distribution functions of the temperature for all the simulations. **Temperature measures the integrated impact of TeV blazar heating over time.** The simulation with the quasar bias model shows significant deviation from the uniform case, especially at lower redshifts. Here the effect of the lower envelope is clear as there is a significant tail toward lower temperatures for $z \leq 3$. **The scatter is strong for the quasar bias mode, where the coldest zones have $T \simeq 10000K$ while the warmest zones have $T \simeq 30000K$ for $z = 3$. The simulation with the quasar bias model shows significant deviation from the uniform case, especially at lower redshifts. Conversely, the warmest gas is only slightly warmer than the mean value and the correspond temperature relatively small. The probability distribution function clearly highlights the impact of clustering on TeV blazar heating.**

To have a better understanding of the heating fluctuations with respect to density fluctuations we represent the mass-weighted $\delta_H - \delta$ distribution on Fig. 6. **The heating rate represents an instantaneous view of the impact of TeV blazar heating. In the quasar bias model (left rows), most of the particles receive slightly more heat than in the uniform case. However, the additional heat is only a few times more than the uniform case. On the contrary, certain regions receive orders of magnitude less heat than the mean value. Certain areas suffer from the decrease of the TeV flux and isolation from massive structures. This is consistent with the temperature probability distribution function presenting an important low temperature tail and**

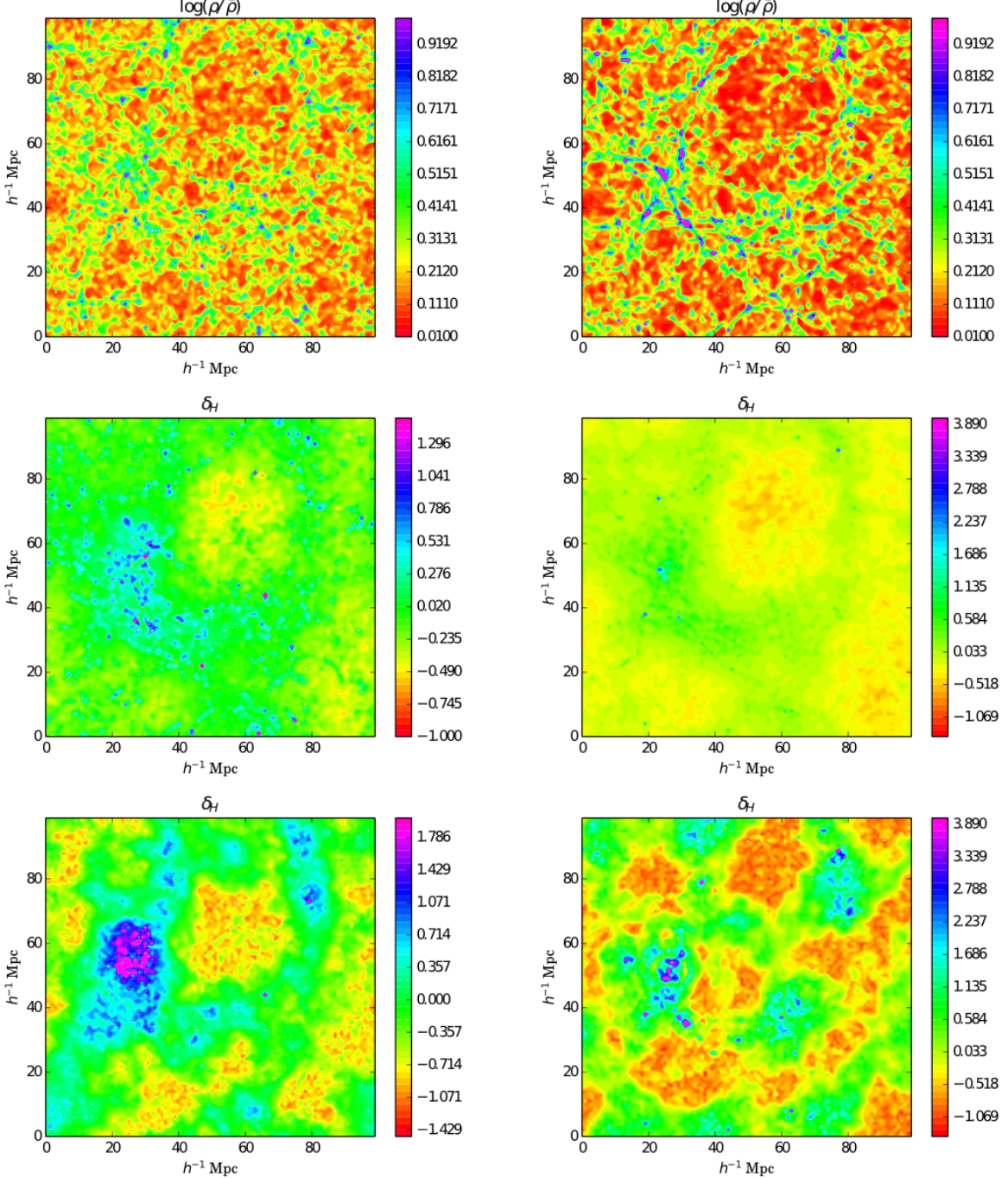


FIG. 2.— Logarithm of the density with respect to the mean value (upper row), heating rate fluctuations with the galaxy (middle row) and quasar model in the $z = 50 h^{-1} \text{Mpc}$ plane. The left column shows $z = 3$, the right one $z = 1$.

a low probability for high temperatures. In the galaxy model, most of the gas has is heated similarly to the uniform case, translating the lower bias for galaxies.

I want to add a 500 Mpc box to model the largest clusters.

5. DISCUSSION

- other heating mechanisms are less efficient
- heat deposited far from sources. complementary to other feedback mechanisms

- compare with uniform model
- linear assumption
- assumption on EBL
- impact of beaming and duty cycle
- uncertainties on bias
- suggest possible applications for window function

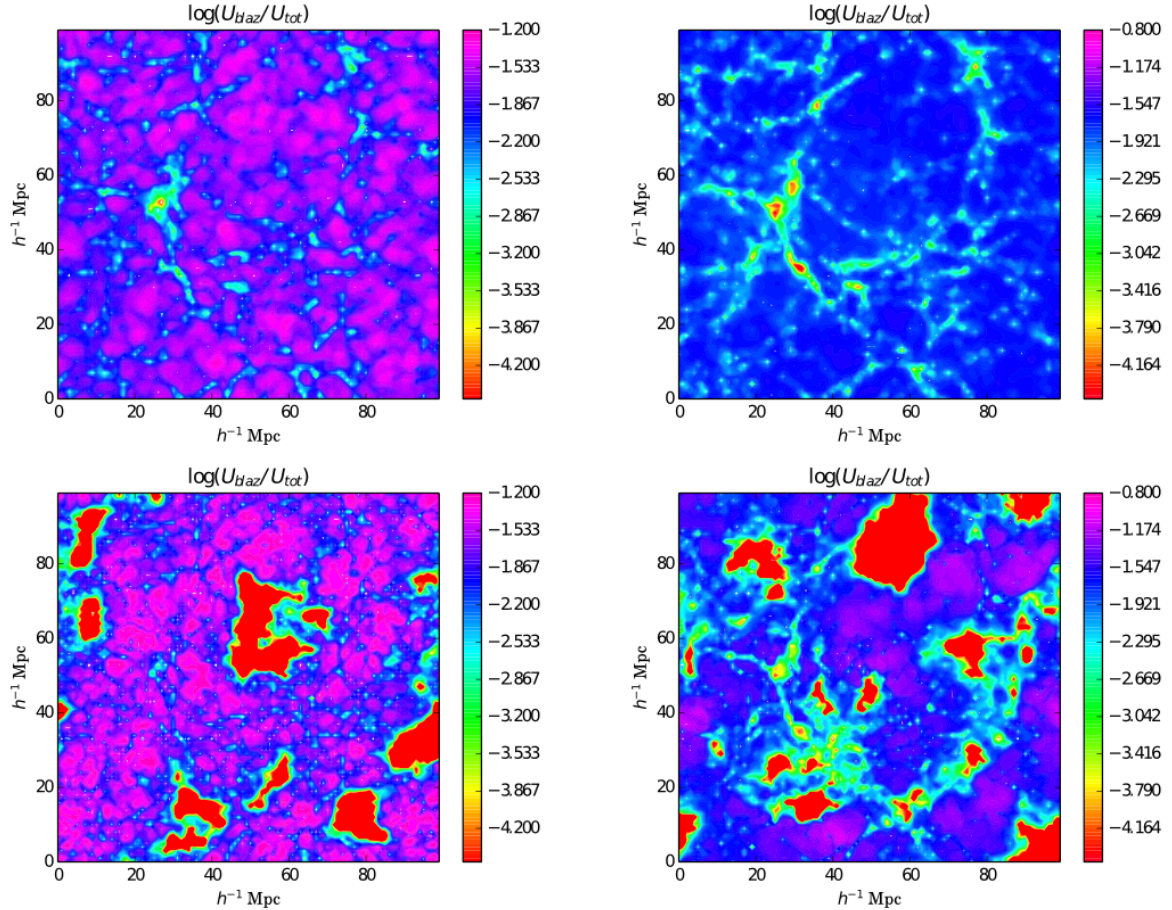


FIG. 3.— Ratio between the energy injection due to blazar heating and the total internal energy **the galaxy bias model (top)** and **the quasar bias model (bottom)** for $z = 3$ (left) and $z = 1$ (right).

- modeling from first principles is impossible. IGM is hard to model and crucial as is the birthplace for galaxies,
- BOSS
- Difficulty to measure T for underdense regions

Detailed modeling of the spectral energy distribution of TeV blazars has enabled to measure the imprint of the EBL and partially constrain its spectrum (H.E.S.S. Collaboration et al. 2013). The EBL is the sum of all the stellar and non-stellar emission throughout the history of the universe and carries important information on the

total star formation. Due to strong foreground emission, direct measurements of the EBL are limited to lower limits (Dole et al. 2006).

6. CONCLUSIONS

This work was supported by the UWM Research Growth Initiative and NSF grant AST-1255469. Simulations were performed using HPC resources from TACC (Grant TG-AST 130004). **Add other grants here. Add Pleiades allocation as well.**

APPENDIX

We detail the derivation of the window function in Eq. 4. We start from a purely Newtonian universe, then include the impact of expansion and finally various first order corrections to the received TeV flux.

NEWTONIAN CASE

Fluctuations with respect to the mean heating rate

The TeV flux received (in photons s⁻¹ cm⁻²) at position \mathbf{x} is given by the sum over all the sources within a radius $r \leq r_{max}$.

$$J(\mathbf{x}) = \int_0^{2\pi} \int_0^{\pi} \int_0^{r_{max}} \frac{\mathcal{E}(\mathbf{x}')}{4\pi|\mathbf{x}' - \mathbf{x}|^2} e^{-\tau} |\mathbf{x}' - \mathbf{x}|^2 \sin \theta d\theta d\phi d(\mathbf{x}' - \mathbf{x}), \quad (\text{A1})$$

where the emissivity \mathcal{E} is given in photons per unit time, per unit volume. $\tau = \kappa(\mathbf{x}' - \mathbf{x})$ is the optical depth along the line of sight, κ the absorption coefficient. Introducing $\mathbf{r}' = \mathbf{x}' - \mathbf{x}$, and $d\Omega = \sin \theta d\theta d\phi$ this gives

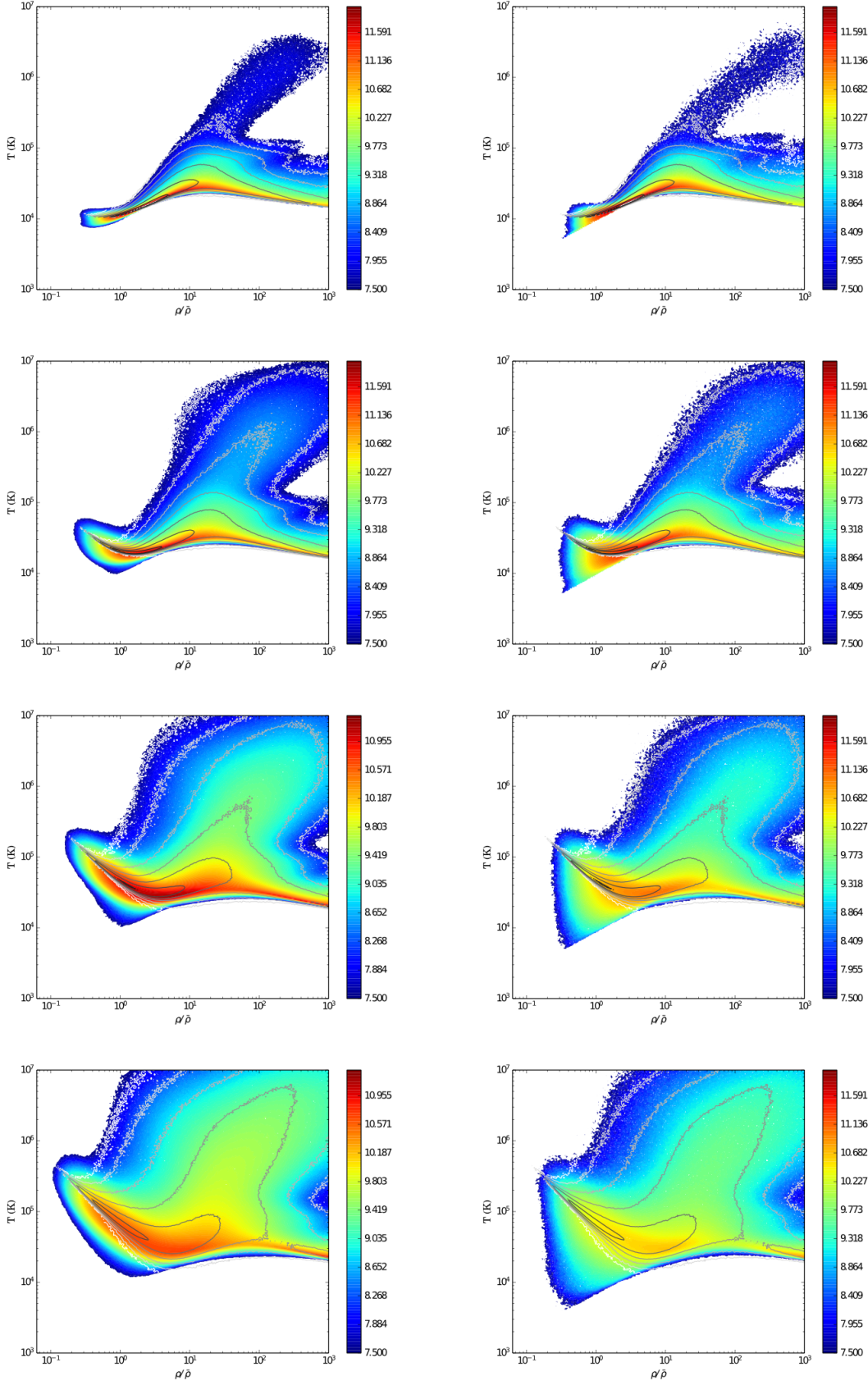


FIG. 4.— Mass weighted temperature - density relation at $z=4,3,2,1$ (from top to bottom) for **the simulations with galaxy bias (left)** and **the quasar bias (right)** The overlying grey contours show the corresponding $T - \rho$ relation for uniform blazar heating (Puchwein et al. 2012) for the same mass range.

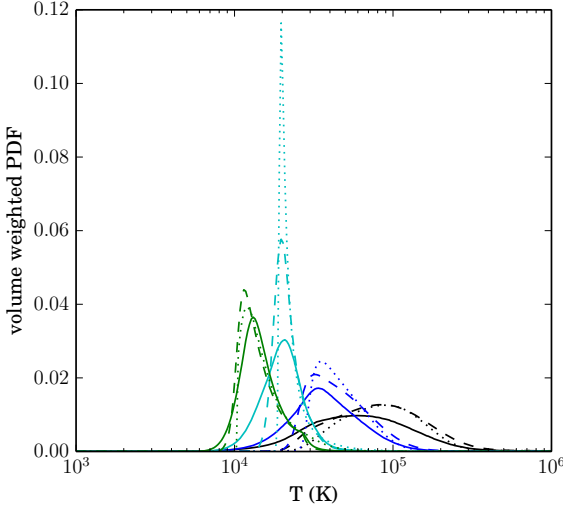


FIG. 5.— Volume-weighted temperature probability distribution function for $z=1$ (black), 2 (blue), 3(cyan) and 4 (green) **for the quasar bias model (solid line), galaxy bias model (dashed line) and the uniform case (dotted line)**.

$$J(\mathbf{x}) = \int_{\Omega} \int_0^{r_{max}} \frac{\mathcal{E}(\mathbf{r}' + \mathbf{x})}{4\pi} e^{-\tau} d\Omega dr'. \quad (\text{A2})$$

The corresponding heating rate ($\text{erg cm}^{-3} \text{ s}^{-1}$) is given by

$$\dot{Q}(\mathbf{x}) = \frac{E_0}{D_{pp}} J(\mathbf{x}) = \frac{E}{4\pi} \int_{\Omega} d\Omega \int_0^{r_{max}} \mathcal{E}(\mathbf{r}' + \mathbf{x}) \frac{1}{D_{pp}} e^{-\tau} dr', \quad (\text{A3})$$

with E_0 the mean energy of the TeV photons and D_{pp} their mean free path before they pair-produce. For convenience reasons, we do not take into account the impact of the spectral energy distribution of the TeV photons in this Appendix. It is taken into account in the exact computation in section §2.

This gives the heating rate per baryon

$$\dot{q}(\mathbf{x}) = \frac{\dot{Q}}{n} = \frac{E_0}{4\pi} \int_{\Omega} \int_0^{r_{max}} \mathcal{E}(\mathbf{r}' + \mathbf{x}) \sigma e^{-\tau} d\Omega dr', \quad (\text{A4})$$

where n is the average density of the target photons (i.e. the EBL) and σ (in cm^{-2}) is the energy averaged cross section for pair production on the extragalactic background light (EBL) photons (Gould & Schréder 1967).

The mean heating rate can be expressed as

$$\bar{q} = \frac{E_0}{4\pi} \int_{\Omega} d\Omega \int_0^{r_{max}} \bar{\mathcal{E}} \sigma e^{-\tau} dr', \quad (\text{A5})$$

with $\bar{\mathcal{E}}$ the mean emissivity. Throughout the whole appendix, barred quantities are spatially averaged quantities.

The heating rate fluctuations at a given point are then given by

$$\begin{aligned} \delta_H(\mathbf{x}) &= \frac{\dot{q}(\mathbf{x}) - \bar{q}}{\bar{q}} = \frac{E_0}{4\pi \bar{q}} \int_{\Omega} d\Omega \int_0^{r_{max}} (\mathcal{E}(\mathbf{r}' + \mathbf{x}) - \bar{\mathcal{E}}) \sigma e^{-\tau} dr' \\ &= \frac{E_0}{4\pi \bar{q}} \int_{\Omega} d\Omega \int_0^{r_{max}} \delta_E(\mathbf{r}' + \mathbf{x}) \bar{\mathcal{E}} \sigma e^{-\kappa r'} dr', \end{aligned} \quad (\text{A6})$$

with the fluctuations in the TeV emissivity δ_E such that one has $\delta_E = \delta$ if the emissivity is directly related to the density.

Window function

As the universe is infinite and asymptotically flat, we can expand the fluctuations into planar waves, in order to get the lengthscale dependence of heating rate fluctuations (Bharadwaj & Ali 2004).

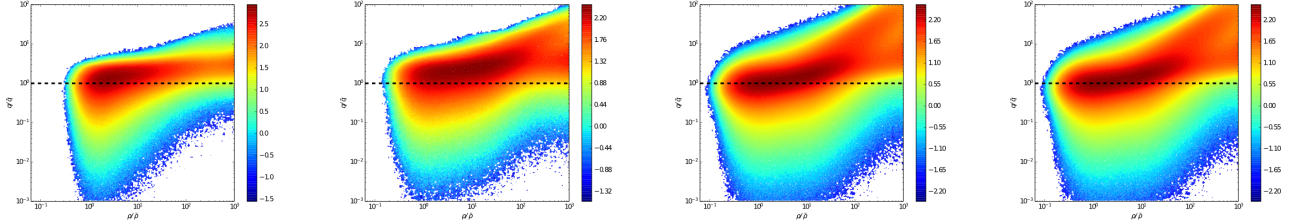


FIG. 6.— Volume-weighted distribution of heating rate fluctuations ($1 + \delta_H$) with respect to the density fluctuations ($1 + \delta$) **for $z=4,3,2,1$ (from left to right)** for the **quasar bias model (left columns)** and the **galaxy bias model (right columns)** at $z=1$ (panel 1 and 3) and $z=3$ (panel 2 and 4). The black dashed line represents the case of uniform blazar heating.

$$\begin{aligned}\delta_H(\mathbf{x}) &= \frac{1}{(2\pi)^3} \int_{-\infty}^{\infty} d^3\mathbf{k}' \tilde{\delta}_H(\mathbf{k}') e^{-i\mathbf{k}' \cdot \mathbf{x}} \\ \delta_E(\mathbf{r}' + \mathbf{x}) &= \frac{1}{(2\pi)^3} \int d^3\mathbf{k}' \tilde{\delta}_E(\mathbf{k}') e^{-i\mathbf{k}' \cdot (\mathbf{r}' + \mathbf{x})},\end{aligned}\quad (\text{A7})$$

Eq. A6 then gives

$$\frac{1}{(2\pi)^3} \int_{-\infty}^{\infty} d^3\mathbf{k}' \tilde{\delta}_H(\mathbf{k}') e^{-i\mathbf{k}' \cdot \mathbf{x}} = \frac{E_0}{4\pi\bar{q}} \int_{\Omega} d\Omega \int_0^{r_{max}} dr' \bar{\mathcal{E}} \sigma e^{-\kappa r'} \frac{1}{(2\pi)^3} \int d^3\mathbf{k}' \tilde{\delta}_E(\mathbf{k}') e^{-i\mathbf{k}' \cdot (\mathbf{r}' + \mathbf{x})}. \quad (\text{A8})$$

Performing an inverse Fourier transform on the right-hand side of Eq.A6, we have

$$\begin{aligned}&= \frac{1}{(2\pi)^3} \frac{E_0}{4\pi\bar{q}} \int_{\Omega} d\Omega \int_0^{r_{max}} dr' \bar{\mathcal{E}} \sigma e^{-\kappa r'} \int d^3\mathbf{k}' \int d^3\mathbf{x} \tilde{\delta}_E(\mathbf{k}') e^{-i\mathbf{k}' \cdot \mathbf{r}'} e^{i(\mathbf{k} - \mathbf{k}') \cdot \mathbf{x}} \\ &= \frac{1}{(2\pi)^3} \frac{E_0}{4\pi\bar{q}} \int_{\Omega} d\Omega \int_0^{r_{max}} dr' \bar{\mathcal{E}} \sigma e^{-\kappa r'} \int d^3\mathbf{k}' \delta^0(\mathbf{k} - \mathbf{k}') e^{-i\mathbf{k}' \cdot \mathbf{r}'} \tilde{\delta}_E(\mathbf{k}') \\ &= \frac{1}{(2\pi)^3} \frac{E_0}{4\pi\bar{q}} \int_{\Omega} d\Omega \int_0^{r_{max}} dr' \bar{\mathcal{E}} \sigma e^{-\kappa r'} \tilde{\delta}_E(\mathbf{k}) e^{-i\mathbf{k} \cdot \mathbf{r}'},\end{aligned}\quad (\text{A9})$$

with $\delta^{(0)}$ the Dirac function, which Fourier transform equals 1. Introducing $\mu = \cos\theta$, where θ is the angle between the wavevector and the line of sight, Eq. A6 rewrites

$$\tilde{\delta}_H(\mathbf{k}) = \frac{E_0}{2\bar{q}} \int_{-1}^1 d\mu \int_0^{r_{max}} \bar{\mathcal{E}} \sigma e^{-\kappa r'} \tilde{\delta}_E(k) e^{-ikr'\mu} dr' \quad (\text{A10})$$

$$\begin{aligned}&= \tilde{\delta}_E(\mathbf{k}) \frac{\sigma E_0}{\bar{q}} \int_0^{r_{max}} \frac{\sin(kr')}{kr'} \bar{\mathcal{E}} e^{-\kappa r'} dr' \\ &= \tilde{\delta}_E(\mathbf{k}) \frac{\sigma E_0}{\bar{q}} \frac{\kappa}{k} \operatorname{atan}\left(\frac{k}{\kappa}\right) \\ &= \tilde{\delta}(\mathbf{k}) \frac{\sigma E_0}{\bar{q}} \frac{\kappa}{k} \operatorname{atan}\left(\frac{k}{\kappa}\right).\end{aligned}$$

(A11)

Fig.7 shows window functions with different absorption coefficients in a purely Newtonian universe. The solid red line shows a case with no absorption, the dashed green line shows a case with $\kappa = 10 \text{ Mpc}^{-1}$. In the former case, large scale structure has the strongest impact on heating, as larger regions have more sources. When absorption is present, the impact of large scale structure (i.e. low k) remains constant as distant sources are absorbed. For scales equal to or larger than the cutoff, heating fluctuations follow density fluctuations and overdense regions get more heat. At smaller scales, the density structure has less impact on the heating, unless a strong overdensity is present.

EXPANDING UNIVERSE

We perform the same derivation as in the former section, replacing the integrals on the (comoving) distance by redshift integrals using

$$dr = \int \frac{c}{H(z)} dz'. \quad (\text{B1})$$

where $H(z)$ is the Hubble parameter.

$$q(\mathbf{z}) = \frac{E_0(1+z)^2}{4\pi} \int_{\Omega} d\Omega \int_z^{z_{max}} \frac{dl}{dz'} \sigma \mathcal{E}(E', z') e^{-\tau} dz'. \quad (\text{B2})$$

$z' = z + \Delta z$, with Δz the difference in redshift between the emission and reception of the photons.

$\mathcal{E}(E', z')$ is the blazar luminosity at the energy E' , which then redshifts to energy E following

$$E' = E \frac{1+z}{1+z'}. \quad (\text{B3})$$

$\tau(E, z', z)$ is the optical depth of a TeV photon observed at redshift z with energy E , which was emitted at redshift z' with energy E' .

$$\tau(E, z', z) = \int_z^{z'} dz'' \frac{1}{D_{pp}} \frac{dl}{dz''} = \int_z^{z'} dz'' \frac{c}{H(z'')} \frac{1}{D_{pp}}, \quad (\text{B4})$$

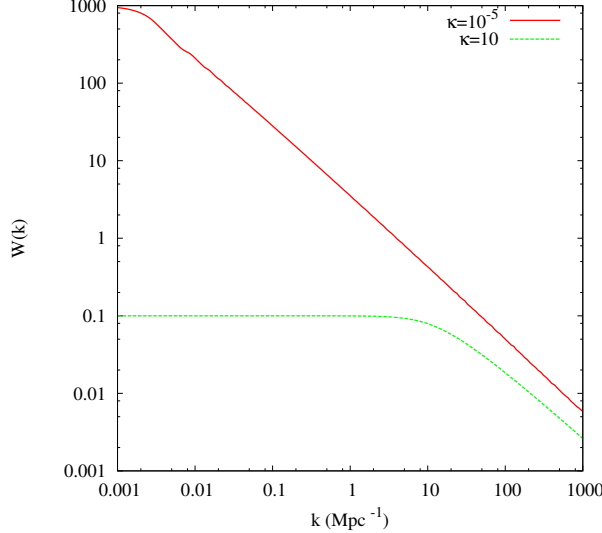


FIG. 7.— Window function for a non-expanding universe. The solid red line has very little absorption ($\kappa = 10^{-5} \text{ Mpc}^{-1}$), the dashed green line has $\kappa = 10 \text{ Mpc}^{-1}$.

Similarly to Eq. A5, the mean heating rate is given by

$$\bar{q} = \frac{E_0(1+z)^2}{4\pi} \int_{\Omega} d\Omega \int \frac{dl}{dz'} \sigma \bar{\mathcal{E}} e^{-\tau} dz'. \quad (\text{B5})$$

The resulting heating rate fluctuations are then given by

$$\begin{aligned} \delta_H(\mathbf{s}) &= \frac{\dot{q}(\mathbf{s}) - \bar{q}}{\dot{q}} = \frac{E_0(1+z)^2 c \sigma}{4\pi \bar{q}} \int_{\Omega} d\Omega \int_z^{z_{max}} \frac{(\mathcal{E}(z') - \bar{\mathcal{E}}) e^{-\tau}}{H(z')} dz' \\ &= \frac{E_0(1+z)^2 \bar{\mathcal{E}} c \sigma}{4\pi \bar{q}} \int_{\Omega} d\Omega \int_0^{z_{max}} \frac{\delta_E(z') e^{-\tau}}{H(z')} dz'. \end{aligned} \quad (\text{B6})$$

The TeV emission is related to the presence of supermassive black holes at the center of galaxies, which are located in collapsed dark matter halos. We can thus connect the fluctuations of the TeV emission, within a certain radius r , to the underlying dark matter fluctuations δ .

At this stage we assume the TeV fluctuations exactly match the dark matter fluctuations $\delta_E = \delta$. We explain in the next section that this is not exactly true and will take into account various corrections. The initial density fluctuations represent a Gaussian random field, which exact properties depend on the earliest stages of the Universe prior to recombination (Bardeen et al. 1986; Peebles 1982). They grow linearly between z' and z following $\delta(z', r) = \delta_0(r)D(z')/D(z)$ (Heath 1977).

$$D(z) = D_0 H(z) \int_z^{\infty} \frac{1+z'}{H^3(z')} dz'. \quad (\text{B7})$$

The linear approximation breaks down when the amplitude of the root mean square of the perturbations approaches unity. The evolution of the density field is then determined by the spherical collapse (Gunn & Gott 1972) and the virialization of halos. As the growth of the modes is independent of the wavenumber, we have

$$\delta_E(z', r) = \delta(z', r) = \delta_0(r)D(z') = \delta_0 D(z') \frac{1}{(2\pi)^3} \int d^3 \mathbf{k}' \tilde{\delta}(\mathbf{k}') e^{-i\mathbf{k}' \cdot \mathbf{r}}. \quad (\text{B8})$$

And Eq. B6 rewrites as

$$\delta_H(\mathbf{s}) = \frac{E_0(1+z)^2 \bar{\mathcal{E}} c \sigma}{4\pi \bar{q}} \int_{\Omega} d\Omega \int_z^{z_{max}} \frac{D(z') \delta(r') e^{-\tau}}{D(z) H(z')} dz'. \quad (\text{B9})$$

The left hand side yields $\tilde{\delta}(\mathbf{k})$ while the right hand side transforms in a similar fashion to Eq. A9. As the power spectrum of density fluctuations is isotropic, this yields

$$\tilde{\delta}_H(k) = \tilde{\delta}(k) \frac{E_0(1+z)^2 \bar{\mathcal{E}} c \sigma}{4\pi \bar{q}} \int_z^{z_{max}} \frac{D(z')}{D(z)} \frac{\sin(kr'(z'))}{kr'(z')} \frac{e^{-\kappa r'(z')}}{H(z')} dz'. \quad (\text{B10})$$

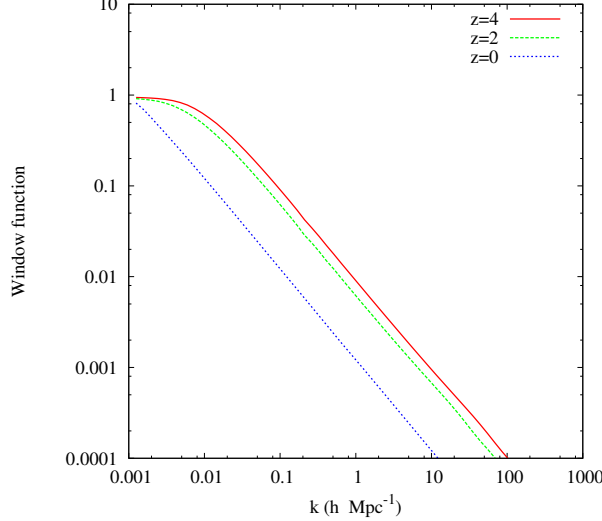


FIG. 8.— Window function in an expanding universe.

Fig. 8 shows the window function in an expanding universe at different redshifts. The TeV emission fluctuations are not exactly equal to the DM density fluctuations. In the next section we will account for the various corrections that have to be taken into account to determine a more accurate window function.

COMPLETE WINDOW FUNCTION

The TeV fluctuations are biased with respect to the dark matter fluctuations, as we detail in § ??, yielding

$$\delta_E = (1 + b(z)\delta) \quad (\text{C1})$$

On top of that, the emitting area (which corresponds to the proper area), evolves as

$$4\pi r(z)^2 = 4\pi r^2 \left(\frac{\bar{\rho}}{\rho(z)} \right)^{2/3} = 4\pi r^2 (\delta(z) + 1)^{2/3}. \quad (\text{C2})$$

A small density perturbation thus gives

$$dA \simeq 4\pi \left(1 + \frac{2}{3}\delta \right) r^2. \quad (\text{C3})$$

If galaxies were moving exactly with the Hubble flow, their redshift would yield their exact distance to an observer. However, galaxies bound to a central potential of a cluster have an infall velocity towards the central overdensity. The proper distance to a source (Eq. B1) then becomes

$$dz' = dr \frac{H(z')}{c} \left(1 - \frac{d\delta_{v_r}(z')}{dr} \right), \quad (\text{C4})$$

where δ_{v_r} are the velocity perturbations along the line of sight. The Fourier transform of δ_{v_r} gives (Kaiser 1987).

$$\mathcal{F} \left(\frac{d\delta_{v_r}}{dr} \right) = -\mu^2 \tilde{\delta}(\mathbf{k}), \quad (\text{C5})$$

with μ the cosine of the angle between the wavenumber and the line of sight.

Keeping only first order correction for density fluctuations, Eq.B2 yields

$$\dot{q}(\mathbf{s}) = \frac{E_0(1+z)^2 c \sigma \bar{\mathcal{E}}}{4\pi} \int_{\Omega} d\Omega \int_z^{z_{max}} \frac{D(z')}{D(z)} \left(1 + \left(b(z) + \frac{2}{3} \right) \delta(r) - \frac{d\delta_{v_r}}{dr} \right) dz'. \quad (\text{C6})$$

Substracting the mean heating rate (Eq. B5) then yields the fluctuations

$$\delta_H(\mathbf{s}) = \frac{1}{X} \int_{\Omega} d\Omega \int_z^{z_{max}} \frac{dX}{dz'} \frac{D(z')}{D(z)} \left(\left(b(z) + \frac{2}{3} \right) \delta(r) - \frac{d\delta_{v_r}}{dr} \right) dz', \quad (\text{C7})$$

where we introduced

$$\frac{dX}{dz'} = \frac{E_0(1+z)^2 \bar{\mathcal{E}} c \sigma}{4\pi} \frac{e^{-\tau(z, z', E')}}{H(z')}, \quad (\text{C8})$$

for convenience reasons and to highlight the generality of the method.

Switching to k -space then yields

$$\begin{aligned} \tilde{\delta}_H(k) &= \frac{1}{X} \int_{\Omega} d\Omega \int_z^{z_{max}} \frac{dX}{dz'} \frac{D(z')}{D(z)} \left(\left(b(z) + \frac{2}{3} \right) \delta(\mathbf{r}' + \mathbf{x}) - \frac{d\delta_{v_r}(\mathbf{r}' + \mathbf{x})}{dr} \right) dz' \\ &= \frac{1}{X} \int_{\Omega} d\Omega \int_z^{z_{max}} \frac{dX}{dz'} \frac{D(z')}{D(z)} \left((b(z) + \frac{2}{3}) \int d^3 \tilde{\delta}(\mathbf{k})' \delta^{(0)}(\mathbf{k} - \mathbf{k}') e^{-i\mathbf{k}' \cdot \mathbf{r}'} \tilde{\delta}(\mathbf{k}') - \int d^3 \mathbf{k}' e^{-\mathbf{k}' \cdot \mathbf{r}'} \delta(\mathbf{k}') \delta^{(0)}(\mathbf{k} + \mathbf{k}') \mu^2 \right) dz' \\ &= \frac{\tilde{\delta}(\mathbf{k})}{X} \int_{-1}^1 d\mu \int_z^{z_{max}} \frac{dX}{dz'} \frac{D(z')}{D(z)} \left((b(z) + \frac{2}{3}) + \mu^2 \right) e^{-ikr\mu} dz' \\ &= \frac{\tilde{\delta}(\mathbf{k})}{X} \int_z^{z_{max}} \frac{dX}{dz'} \frac{D(z')}{D(z)} \left((b(z) + 1) j_0(kr) - \frac{2}{3} j_2(kr) \right) dz'. \end{aligned} \quad (\text{C9})$$

With the spherical Bessel functions

$$j_0(kr) = \frac{\sin(kr)}{kr} \quad (\text{C10})$$

$$j_2(kr) = \left(\frac{3}{x^2} - 1 \right) \frac{\sin(x)}{x} - \frac{3\cos(x)}{x^2}. \quad (\text{C11})$$

We have used

$$\int_{-1}^1 \mu^2 e^{ikr\mu} d\mu = \frac{2\sin(kr)}{kr} + 4 \frac{\cos(kr)}{(kr)^2} - 4 \frac{\sin(kr)}{(kr)^3}. \quad (\text{C12})$$

The window function for the heating rate fluctuations is then given by

$$\tilde{W}_H(k, z) = \frac{E_0(1+z)^2 \sigma c \bar{\mathcal{E}}}{4\pi \bar{q}} \int_z^{z_{max}} \frac{e^{-\tau}}{H(z')} \frac{D(z')}{D(z)} \left((b(z) + 1) j_0(kr) - \frac{2}{3} j_2(kr) \right) dz'. \quad (\text{C13})$$

Which is the same window function as Pritchard & Furlanetto (2007); Barkana & Loeb (2005).

REFERENCES

- Aleksić, J., Antonelli, L. A., Antoranz, P., et al. 2010, A&A, 524, A77
- Bardeen, J. M., Bond, J. R., Kaiser, N., & Szalay, A. S. 1986, ApJ, 304, 15
- Barkana, R., & Loeb, A. 2005, ApJ, 626, 1
- Basilakos, S., Plionis, M., & Ragone-Figueroa, C. 2008, ApJ, 678, 627
- Bharadwaj, S., & Ali, S. S. 2004, MNRAS, 352, 142
- Boera, E., Murphy, M. T., Becker, G. D., & Bolton, J. S. 2014, MNRAS, 441, 1916
- Bolton, J. S., Becker, G. D., Haehnelt, M. G., & Viel, M. 2014, MNRAS, arXiv:1308.4411
- Bolton, J. S., Viel, M., Kim, T.-S., Haehnelt, M. G., & Carswell, R. F. 2008, MNRAS, 386, 1131
- Bond, J. R., Kofman, L., & Pogosyan, D. 1996, Nature, 380, 603
- Bret, A., Firpo, M.-C., & Deutsch, C. 2004, Phys. Rev. E, 70, 046401
- Broderick, A. E., Chang, P., & Pfrommer, C. 2012, ApJ, 752, 22
- Chang, P., Broderick, A. E., & Pfrommer, C. 2012, ApJ, 752, 23
- Clowes, R. G., Harris, K. A., Raghunathan, S., et al. 2013, MNRAS, 429, 2910
- Cooray, A., & Sheth, R. 2002, Phys. Rep., 372, 1
- Croom, S. M., Boyle, B. J., Shanks, T., et al. 2005, MNRAS, 356, 415
- Dermer, C. D., Cavadi, M., Razzaque, S., et al. 2011, ApJ, 733, L21
- Dole, H., Lagache, G., Puget, J.-L., et al. 2006, A&A, 451, 417
- Durrer, R., & Neronov, A. 2013, A&A Rev., 21, 62
- Faucher-Giguère, C.-A., Lidz, A., Zaldarriaga, M., & Hernquist, L. 2009, ApJ, 703, 1416
- Franceschini, A., Rodighiero, G., & Vaccari, M. 2008, A&A, 487, 837
- Gould, R. J., & Schréder, G. P. 1967, Physical Review, 155, 1408
- Gunn, J. E., & Gott, III, J. R. 1972, ApJ, 176, 1
- H. E. S. S. Collaboration, Abramowski, A., Aharonian, F., et al. 2014, ArXiv e-prints, arXiv:1401.2915
- Heath, D. J. 1977, MNRAS, 179, 351
- H.E.S.S. Collaboration, Abramowski, A., Acero, F., et al. 2013, A&A, 550, A4
- Hockney, R. W., & Eastwood, J. W. 1981, Computer Simulation Using Particles
- Hopkins, P. F., Richards, G. T., & Hernquist, L. 2007, ApJ, 654, 731
- Kaiser, N. 1987, MNRAS, 227, 1
- Kashikawa, N., Yoshida, M., Shimasaku, K., et al. 2006, ApJ, 637, 631
- Kauffmann, G., Colberg, J. M., Diaferio, A., & White, S. D. M. 1999, MNRAS, 307, 529
- Kneiske, T. M., Bretz, T., Mannheim, K., & Hartmann, D. H. 2004, A&A, 413, 807
- Komatsu, E., Smith, K. M., Dunkley, J., et al. 2011, ApJS, 192, 18
- Kravtsov, A. 2010, Advances in Astronomy, 2010, arXiv:0906.3295
- Mann, R. G., Peacock, J. A., & Heavens, A. F. 1998, MNRAS, 293, 209
- Marinoni, C., Le Fèvre, O., Meneux, B., et al. 2005, A&A, 442, 801
- Miniati, F., & Elyiv, A. 2013, ApJ, 770, 54
- Mo, H. J., & White, S. D. M. 1996, MNRAS, 282, 347

- Myers, A. D., Brunner, R. J., Nichol, R. C., et al. 2007, ApJ, 658, 85
- Neronov, A., & Semikoz, D. V. 2009, Phys. Rev. D, 80, 123012
- Peebles, P. 1982, Principles of Physical Cosmology, ed. T. Anderson, Wightman (Princeton University Press)
- Pfrommer, C., Chang, P., & Broderick, A. E. 2012, ApJ, 752, 24
- Pontzen, A. 2014, Phys. Rev. D, 89, 083010
- Pritchard, J. R., & Furlanetto, S. R. 2007, MNRAS, 376, 1680
- Puchwein, E., Pfrommer, C., Springel, V., Broderick, A. E., & Chang, P. 2012, MNRAS, 423, 149
- Rauch, M., Miralda-Escude, J., Sargent, W. L. W., et al. 1997, ApJ, 489, 7
- Ricotti, M., Gnedin, N. Y., & Shull, J. M. 2000, ApJ, 534, 41
- Rudie, G. C., Steidel, C. C., & Pettini, M. 2012, ApJ, 757, L30
- Saveliev, A., Evoli, C., & Sigl, G. 2013, ArXiv e-prints, arXiv:1311.6752
- Schaye, J., Theuns, T., Rauch, M., Efstathiou, G., & Sargent, W. L. W. 2000, MNRAS, 318, 817
- Schlickeiser, R., Ibscher, D., & Supsar, M. 2012, ApJ, 758, 102
- Schlickeiser, R., Krakau, S., & Supsar, M. 2013, ApJ, 777, 49
- Shen, Y., Strauss, M. A., Oguri, M., et al. 2007, AJ, 133, 2222
- Simionescu, A., Werner, N., Böhringer, H., et al. 2009, A&A, 493, 409
- Sironi, L., & Giannios, D. 2014, ApJ, 787, 49
- Springel, V. 2005, MNRAS, 364, 1105
- Springel, V., & Hernquist, L. 2002, MNRAS, 333, 649
- . 2003, MNRAS, 339, 289
- Stecker, F. W., de Jager, O. C., & Salamon, M. H. 1992, ApJ, 390, L49
- Stecker, F. W., Malkan, M. A., & Scully, S. T. 2006, ApJ, 648, 774
- Tegmark, M., Blanton, M. R., Strauss, M. A., et al. 2004, ApJ, 606, 702
- Viel, M., Bolton, J. S., & Haehnelt, M. G. 2009, MNRAS, 399, L39
- Viel, M., Haehnelt, M. G., & Springel, V. 2004, MNRAS, 354, 684
- Vovk, I., Taylor, A. M., Semikoz, D., & Neronov, A. 2012, ApJ, 747, L14
- Weinberg, D. H., Davé, R., Katz, N., & Hernquist, L. 2004, ApJ, 601, 1
- Werner, N., Simionescu, A., Million, E. T., et al. 2010, MNRAS, 407, 2063